Zero-staging the Aero-derivative Marine Gas Turbine for a Step-Change Increase in Power Rating.

Ronald Portanier[1]
University of Plymouth - MLA College
ronaldportanier@hotmail.com

Synopsis

Navies that sought to upgrade their fleet's mission capability and increase their on-board load usually resorted to increasing the ship's propulsive power. When the ship's prime mover was a gas turbine, this could be done by zero-staging the existing gas turbine compressor. An aero-derivative gas turbine for marine propulsion was a prime candidate for zero-staging because it retained its original attributes of high power-to-weight ratio, compactness, fast start-up, and variable power output. A successful zero-staged compressor gave a step-increase in power with minimal changes to the original inlet while keeping the remainder of the installation intact. As a result, the development costs were relatively less when compared to a new replacement design with a higher power rating. The purpose of this paper is to discuss a zero-staged design method for an aero-derivative marine gas turbine for an improvement in performance and an increase in power output. Here, a sequential approach was taken when carrying out the synthesis, with the completion of each sequence serving as a gate keeper prior to proceeding to the next sequence. This resulted in the formulation of a method that assessed the feasibility of zero staging the gas turbine at the initial design phase by applying basic calculations. The simplicity of the proposed method permitted the sole use of a spreadsheet instead of the established practice of complex numerical analyses with extensive batch data processing on a computer server. The intent was to ensure the viability of the zero-stage design at the preliminary investigative phase in a simplistic manner prior to committing to a fully-fledged design project of significant cost. This approach was used as a case study on an existing medium-size aero-derivative gas turbine suitable for marine use–namely the Rolls-Royce Trent 60 Siemens SGT-A65 gas turbine. Zero-staging gave a 17% increase in power output, from 57.4 MW to 67.1 MW.

Key words: *marine propulsion; gas turbine engine; power uprate; zero-staging.*

1. Introduction

A ship that had to maximize its capability, increase its on-board load or change its area of operation from a low to a high wave condition, for example, from an enclosed sea to an open ocean, would resort to an increase in propulsion power for its new operational profile. If the ship's prime mover was a gas turbine, the gas turbine manufacturer would usually be asked to provide a power upgrade by increasing the gas turbine's gas path for a higher air flow capacity. This meant that the gas path components had to be redesigned to the larger annulus. This became a major undertaking that carried a high development cost.

It was possible to obtain a higher power output by zero-staging the ship's existing gas turbine. Zero-staging meant that the compressor had an added stage at the front that raised the compressor pressure ratio. This permitted more fuel flow to the combustor and a resulting increase in shaft power output. Zero-staging became a viable solution because it enhanced the gas turbine's high power-to-weight density, kept its compactness and light weight, and maintained its very fast start and rapid variable power output. Zero-staging was particularly beneficial for an existing gas turbine because the remainder of the gas path was not changed, thus keeping the original components. It also permitted the existing gas turbine installation interfaces to be retained. As a result the costs were significantly less when compared to having a new gas turbine of equivalent higher power.

Synthesizing the zero-stage design required applying those design rules that were determinant to the gas turbine's performance parameters. The design synthesis entailed composing the compressor map at the higher pressure to make sure there was sufficient surge margin, confirming that in the least, the thermal efficiency was retained, determining that the increase in turbine temperature could be tolerated, defining the zero-stage rotor and stator airfoil geometry, ensuring the rotor passing frequencies for the compressor first stages were not damaging, confirming that the alarm levels and trip limits were not worse, and finally estimating the higher power output.

These were all done in a sequential manner, with each sequence completed prior to proceeding to the next sequence. The intent was to develop a simple and straight-forward method that became applicable in a generic sense. This simplicity permitted a single person using a spreadsheet to synthesize the zero-stage design. The method developed ensured that the zero-stage design was of merit during the initial assessment and prior to

---

[1] Ronald Portanier CEng, CMarEng, FIMarEST, PhD, worked at Pratt & Whitney Canada, Roll-Royce Canada and Siemens Canada, carrying out gas turbine centre-line designs and leading R&D projects. His roles encompassed subject expert where he obtained patents on gas turbine designs and project lead. He recently completed an MSc Engineering at MLA College.

committing expensive resources that involved subject experts and complex numerical analysis that required data processing with a computer server.

This method was tried as a case study by assessing the feasibility of zero-staging the Rolls-Royce Trent 60 Siemens SGT-A65 gas turbine. The Trent 60 was an aero-derivative version of the Rolls-Royce Trent 800 aero-fan gas turbine. The Trent 60 configuration retained the three-spool architecture of the Trent aero-fan engine but had its own low pressure compressor and low pressure turbine. Its three-spool architecture permitted it to keep the aero-characteristics of the Trent 800 for rapid shaft power maneuverability. It also ran on Diesel fuel, making it affordable to operate. Its compactness gave it a high power density that made it ideal as a marine propulsion engine. In addition, its small size permitted an easy change out and its modular build made it amenable for on board maintenance by splitting the casings and changing out parts. By virtue of its configuration, it became an appropriate candidate for having a zero-stage design because it did not disturb the remainder of the configuration.

Figure 1 shows a cross-section representation of the existing Trent 60 gas turbine as a mechanical drive. Viewing the image from left to right, we have the air inlet, the low pressure, intermediate pressure and high pressure compressors, the combustor, and the high pressure, intermediate pressure and low pressure turbines and exhaust, with the output drive shaft along the centre-line. The numbers *1*, *2*, *3 3'*. *4* and *4'* indicate the thermodynamic points along the gas path.

$1=T_{inlet}$; $2=T_{compressor}$; $3=T_{combustor}$; $3'=T_{turbine}$; $4=T_{exhaust}$; $4'=T_{exhaust\ duct}$.
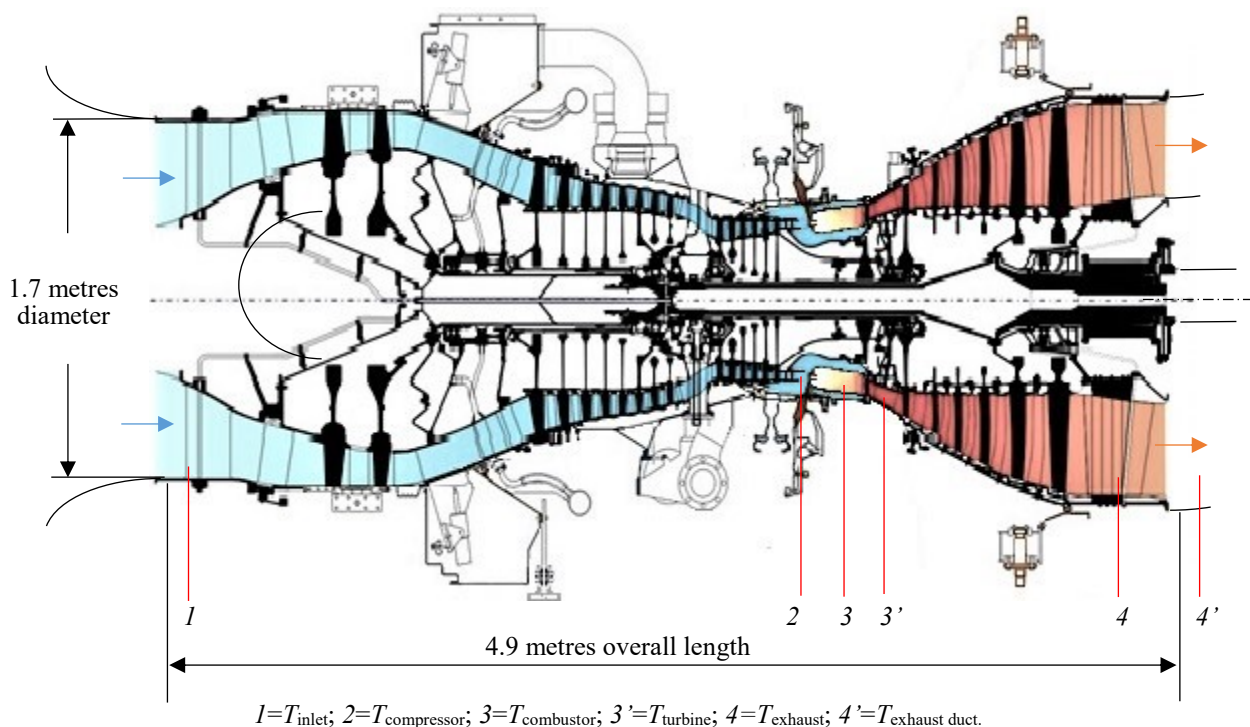
Figure 1. Rolls-Royce Trent 60 Siemens SGT-A65 Cross-Section (Rolls-Royce. Siemens)

2. Objective

The objective of this paper was to discuss the synthesis of a zero-stage power upgrade to an existing gas turbine engine and how this could be done in a simplified manner without degrading the quality of the analysis. The intent was to show how this simple method could be applied during the investigative phase of the zero-stage design. The primary considerations for zero-staging the gas turbine were identified and these became the target requirements for the zero-staged assessment. These were:
- The gas turbine configuration and gas path were to remain the same except for the added zero-stage.
- The effect of zero-staging would cause the compressor design point to shift upward, thus maintaining thermal efficiency.
- There was to be sufficient compressor surge margin.
- The increase in the turbine firing temperature could be tolerated.
- The rotor passing frequencies were not damaging.
- The alarms and limits were not to be worse.
- The higher torque due to the increase in power output could be met.

3.   Methodology

The approach taken for carrying out the zero-stage synthesis consisted in determining the thermodynamic, aerodynamic and mechanical integrity requirements and from these conceptualizing the zero-stage geometrical definition for an increase in compressor pressure and fuel consumption, and a higher power output. To synthesize the zero-stage design, use was made of basic gas turbine text book equations that were then applied for a specific calculation. Here, the method consisted in a sequential approach, with the results from each sequence compared to the expected outcome and serving as a gate keeper prior to proceeding to the next step. The method was purposely kept simple so that it could be used at the initial design phase in an expedient manner. The methodology developed became applicable in a generic sense for zero-staging an existing gas turbine.

4.   Findings

4.1.   *Zero-staging Thermodynamic Assessment*

The first requirement consisted in determining the capability of the gas turbine to accommodate an increase in power relative to its standard rating. This required comparing the aero-derivative gas turbine's existing thermodynamic points to their parent aero-fan gas turbine counterparts to establish if there was any margin. The compressor, combustor and turbine temperature points $1 = T_{inlet}$; $2 = T_{compressor}$; $3 = T_{combustor}$; $3' = T_{turbine}$; $4 = T_{exhaust}$; and $4' = T_{exhaust\ duct}$ of Figure 1 were compared by applying the proportionality relationships. This comparison was possible because the aero-derivative gas turbine had the same core as the aero-fan gas turbine with the only difference being their operating parameters (EASA, 2019) (Jackson, 2009) (Siemens SGT-A65, 2018). Equation (1) and Equation (2) below represent the aero-fan temperatures on the left and the aero-derivative temperatures on the right:

$$\text{Aero-fan } (T_{compressor} / T_{combustor}) = \text{Aero-derivative } (T_{compressor} / T_{combustor}) \qquad (1)$$

$$\text{Aero-fan } (T_{combustor} / T_{turbine}) = \text{Aero-derivative } (T_{combustor} / T_{turbine}) \qquad (2)$$

The results showed that the aero-derivative core was operating at a lower temperature than its aero-fan counterpart by 4% (Table 1). This was expected because the Trent 60 was running at a lower pressure ratio of 34.3, which was 2% less when compared to the Trent 800 that was operating at a pressure ratio of 35. Hence, there was scope to increase the power output of the Trent 60 because there was room for a temperature increase.

Although it was possible to attain a higher power rating with a simple throttle push, this would result in the gas turbine running off-design with a loss of thermal efficiency. Hence the preferred solution was to raise the working line by zero-staging. However, the viability of zero-staging also depended on how much more temperature the gas turbine could endure.

4.2.   *Thermal Efficiency Analysis*

The next step required determining the gas turbine's thermal efficiency. This was set by the turbine temperature limit. Current blade cooling technology was deemed adequate for a turbine e ntry temperature of 1,800 K for the aero-fan Trent turbine (Jackson, 2009). It was possible for the turbine to tolerate an entry temperature of 1,815 K by improving its cooling (Portanier, 2021). Hence, this temperature was referenced as the upper limit for a zero-stage operation at maximum power.

The thermal efficiency for the existing aero-derivative configuration was calculated from Equation 3 by Boyce (2011).

$$\eta_{cycle} = \left(\frac{\eta_t T_f - \dfrac{T_{amb}\, r_p^{\frac{(\gamma-1)}{\gamma}}}{\eta_c}}{T_f - T_{amb} - T_{amb} \left(\dfrac{r_p^{\frac{(\gamma-1)}{\gamma}} - 1}{\eta_c} \right)} \right) \left(1 - \frac{1}{r_p^{\frac{(\gamma-1)}{\gamma}}} \right) \qquad (3)$$

Here η_{cycle} = the thermal efficiency; r_p = the pressure ratio = 34.3; $T_{ambient}$ = the ambient temperature = 288.15 K; γ = the specific heat ratio = 1.4; T_f = the turbine firing temperature = 1,622 K, obtained by Equation (2); n_c = the compressor efficiency = 0.86; and η_t = the turbine efficiency = 0.89. The efficiency values were from Jackson (2009).

The specific heat ratio for γ was given as the standard value for air. Its value was affected by the temperature and would be reduced as the air flowed through the compressor and noticeably more as the air flowed through the turbine. From the low pressure compressor to the high pressure compressor, γ reduced to approximately 1.37, and for the turbine averaged 1.33 (Jackson, 2009). However, a value of $y = 1.4$ was purposely kept throughout this calculation to keep it simple for this preparatory phase of the assessment.

Applying the above values to Equation (3) gave the thermal efficiency for the existing Trent 60 as 43.9%. The gas turbine manufacturer guaranteed the thermal efficiency of the Trent 60 as 43.6% (Siemens SGT-A65, 2018). This was in line with the result from Equation (3). Although Equation (3) was intended for a single spool gas turbine and not a three spool configuration, it served the initial purpose of assessing the validity of the turbine firing temperature calculation.

The next step was to determine the thermal efficiency up to the maximum possible turbine firing temperature of 1,815 K, which was made limiting as previously stated. The thermal efficiency was calculated up to the higher turbine temperature (Table 2). This showed a possible thermal efficiency increase to 46.8%, or by 2.9%, up to a pressure ratio of 38.1 (Table 3). This result did not mean that the configuration of the gas turbine could arbitrarily accommodate a higher pressure. Further analysis was needed.

4.3. Mass Flow Analysis

The next step was to ascertain if the increase in mass flow as a result of the higher pressure ratio was limiting. The higher mass flow was calculated using the expression from Walsh (2004):

$$Q = W \sqrt{T} / P \tag{4}$$

Here Q was the flow coefficient, W was the mass flow, T was the compressor temperature and P was the compressor pressure. The value of Q was first established for the pressure ratio of 34.3 with $W = 157.7$ kg/second. This permitted repeating the calculation up to a compressor pressure ratio of 38.1 (Table 4). The results showed a potential increase in mass flow up to 192.8 kg/second. The gas turbine manufacturer gave an exhaust mass flow of 178 kg/second when the Trent 60 was used to drive an electrical power generator at continuous steady state (Siemens SGT-A65, 2018). Although it was possible to have a compressor pressure ratio of 38.1, the mass flow of 192.8 kg/second exceeded the gas turbine manufacturer's continuous power rating of 178 kg/second. As a consequence, a mass flow of 178 kg/second was used to quantify the thermal efficiency benefit at zero-staging conditions. This mass flow required a compressor pressure ratio of 36.8 and this value was used for assessing the zero-stage baseload operation.

The Trent 60 as an aero-derivative mechanical drive gas turbine was rated for a power overspeed of 5% (Siemens SGT-A65, 2018). There was scope for a 5% power overspeed as part of the zero-stage uprate provided a higher mass flow could be accommodated. The gas turbine as a marine propulsion engine would operate at this higher rating when it required a torque boost. This is reviewed later when compressor mapping is discussed.

4.4. Compressor Efficiency Analysis

The viability of zero-staging the compressor required knowing the new compressor efficiency. This was calculated at steady state base load conditions. The original isentropic compressor efficiency was determined from the equation by Boyce (2011):

$$\eta_c = (r_p^{(0.2857)\,\eta\text{ polytropic}} - 1) / (r_p^{(0.2857)} - 1) \tag{5}$$

The polytropic efficiency $\eta_{\text{polytropic}}$ used was 91% and was obtained from Walsh (2004). The efficiency came to 86.33%. The original compressor isentropic efficiency was given by Jackson (2008) as $\eta_c = 86\%$. This confirmed the suitability of Equation (5).

The new compressor efficiency for the pressure ratio of 36.8 with the rated mass flow of 178 kg/second was calculated using Equation (5). This came to 86.22%. This very small difference when compared to the 86.33% efficiency for a pressure ratio of 34.3 indicated that the higher pressure ratio was not detrimental to the compressor's aerodynamic response. This meant that increasing the compressor pressure ratio to 36.8 was aerodynamically feasible. The same calculation was repeated for the 5% overspeed condition with a pressure ratio of 38.1 and a corresponding mass flow of 192.8 kg/second. This gave a compressor efficiency of 86.18%. This small difference also indicated that this higher speed was not detrimental to the compressor's aerodynamic response.

The compressor exit temperature at station 2 in Figure 1 for an original pressure ratio of 34.3 was 873 K (Siemens SGT-A65, 2018). The temperature as a result of the higher pressure ratio of 36.8 was calculated to be 891 K. This was 19 K less than the aero fan compressor exit temperature of 910 K (EASA, 2019). Hence, the

compressor could operate suitably with a mass flow rating of 178 kg/second. When the pressure ratio was increased to 38.1, for the higher mass flow of 192.8 kg/second and the higher compressor temperature of 901 K, the compressor would be able to tolerate this higher temperature because it was below the aero-fan temperature values. On the basis of the result obtained so far, there was scope to zero-stage the gas turbine compressor.

4.5.   Compressor Aerodynamic Assessment

The next phase of the assessment consisted in plotting the compressor map with a super-imposed zero stage and a 5% overspeed condition. The intent was to define the higher pressure working line and the stall and choke limits, especially when running off design during start-up and shut-down.

The compressor map was usually plotted by the gas turbine manufacturer by carrying out a compressor rig test. At this early phase, this was not deemed justifiable because it required an actual compressor test facility and involved considerable cost. Rather, a simplified method was developed with all three compressors considered as a single spool and with the inner and outer hade angles of the three compressors taken to be equal, while in reality the Trent 60 had separately profiled gas paths for each of the three compressor spools as shown in Figure 1.

The end points for plotting the compressor working line used the compressor inlet pressure and air flow as the lower limits, and the maximum compressor exit temperature and air flow as the upper limits. The analysis for plotting the map treated each stage separately for the sixteen stages of the original configuration, plus the added zero-stage and a fictitious eighteenth stage for the overspeed conditions, for a total of eighteen stages (Table 5). Each stage was analyzed for its own pressure ratio and mass flow. This was next done by rotor speed (Table 6). This resulted in being able to plot the working line incrementally up the power curve.

The rotor speed was next drawn at each intersection as a parabolic curve with the vertical and horizontal ends of the parabola determining the stall point and choke point, respectively. The result showed the viability of increasing the pressure ratio, namely because the surge margin was retained, even at the 5% overspeed. Figure 2 shows the compressor map plotted by this method.
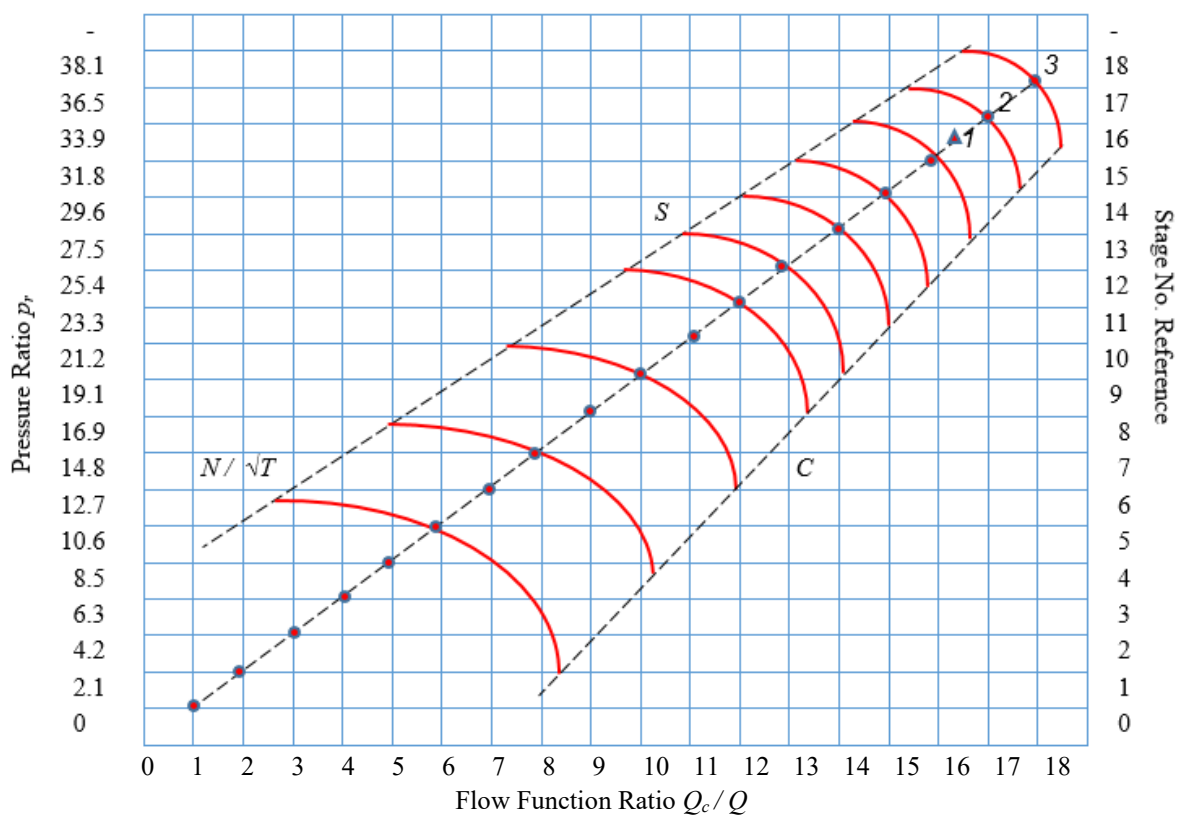
▲*1* denotes the original design point for flow $W = 157.7$ kg/second at $r_p = 34.3$.
●*2* denotes the calculated projection for flow $W = 185.34$ kg/second at $r_p = 36.5$.
●*3* denotes the calculated projection for the 5% overspeed.
S is the assumed stall line. *C* is the assumed choke line.

Figure 2. Hypothetical Compressor Aero-Dynamic Map.

4.6. Zero-Stage Gas Path Definition

The next step was to ascertain that the zero-stage configuration was able to be accommodated as an extension of the gas path to form part of the compressor front end. This required defining the gas path geometry of the zero stage. The inner and outer annuli were a straightforward forward extension of the gas path of the first stage, but the size of the annulus at the inlet plane and the added extension to the gas path needed quantifying.

This required calculating the pitch line blade speed and radius. At this initial phase, the inner and outer hade angles of the compressor were taken to be equal so that the pitch line was the same throughout the entire axial length of the compressor. This permitted determining the pitch radius of the zero-stage blade in a simplistic manner without having to consider every stage of the compressor.

The blade speed was first calculated using the stage loading equation from Walsh (2004):

$$\text{Stage loading} = \frac{C_p \left(T_{compressor} - T_{ambient} \right)}{\left(\text{blade pitch speed}^2 \text{ x number of stages} \right)} \tag{6}$$

Here, $Cp = 1.006$ kJ/kg, $T_{compressor} = 891$ K as previously calculated, $T_{ambient} = 288.15$ K, and with 17 stages, that is with the added zero-stage.

Three stage loading values were considered. These were 0.3, 0.35 and 0.4. The pitch radius was calculated from:

$$\text{Blade pitch speed} = \text{blade pitch radius x } 2\pi \text{ / 60 x blade speed} \tag{7}$$

The blade speed was based on a shaft speed of 3,570 rpm, as stated in the Trent 60 data sheet (Siemens SGT-A65 2018). A stage loading of 0.4 gave the best fit in the gas path's available space with a blade speed of 298 metres/second and a resulting pitch radius of 799 mm.

The size of the annulus was next considered. This required knowing the inlet Mach number. The axial inlet velocity relative to the row of rotating blades ventured towards supersonic for the upper part of the blade, towards subsonic for the lower part, and with the mean value taken as transonic (Cohen *et al.*, 1972). For this initial assessment only the mean value was analysed. Here, a Mach number of 0.4 was considered as typical for the inlet flow condition (Portanier, 2021). Walsh (2004) provided a look-up table for a range of Mach numbers for their respective temperature, pressure and flow function.

From the table by Walsh (2004), for a Mach number of 0.4, the static flow function was given as $q = 25.41$. Applying:

$$q = (\text{mass flow } W) \, (T_{ambient}) \, r_p^{1/2}) \, (\text{annulus area } A) \, (P_{ambient}) \tag{8}$$

and with $W = 157.7$ kg/second and $r_p = 34.3$, the annulus area A was found to be 1.0523 m^2.

Knowing the annulus area and the inlet outer diameter of 1,700 mm in Figure 1 permitted determining the blade height from:

$$\text{Area } A = \pi \left(R_{tip}^2 - R_{hub}^2 \right) \tag{9}$$

For a tip radius $R_{tip} = 1,700/2$ mm $= 850$ mm, the hub radius R_{hub} came to 641 mm. That is, the throat of the calculated annulus allowed a blade height of 850 mm - 641 mm = 209 mm. To compensate for airflow inefficiency, the blade height was increased by 5% from 209 mm to 220 mm (Jahanmiri, 2011).

One more calculation was needed to determine the protrusion of the gas path as a result of adding the zero-stage. This entailed defining the chord lengths for the zero-stage vane and blade and adding a 20% gap in between. This gap was set to minimize downstream vibratory effects from the blade and avoid clipping. Here, the chord length was determined from the chord aspect ratio defined as height/chord. Based on best design practices for compressor fans and blades this varied from 2.0 to 3.5 and for vanes it was 2.5 (Walsh, 2004). Large low pressure compressor blades approximated fan blades in their aerodynamic behaviour and a chord aspect ratio of 2.0 was applied.

Hence, for a hypothetical blade height of 220 mm the chord length came to 220 / 2 = 110 mm. If the vane height had the same value, the chord length would be 220 / 2.5 = 88 mm.

The gas path extension was calculated for both chord lengths, and by adding the mandatory 20% gap in between, this came to 238 mm. This extension together with the larger frontal annulus could be suitably accommodated by slightly flaring out the inner profile of the gas path.

4.7. Airfoil Count

The airfoil count next needed to be established. From a blade chord lengths of 110 mm and a vane chord length of 88 mm and from the standard velocity triangles with the angle ratios at the mean blade height, α_1 / α_2 and β_2 / β_1 taken as 0.80, the blade pitch was determined as s_{blade} = 0.80 x 110 mm = 88 mm and the vane pitch was determined as s_{vane} = 0.80 x 88 mm = 70.4 mm. From the blade mean radius R = 712.18 mm, the blade and vane counts came to n_{blade} = 2 π R / 88 = 51 and n_{vane} = 2 π R / 70.4 = 64.

It was practice to have the stator with an even number of airfoils and the rotor with a prime number of airfoils (Cohen *et al*., 1972). Hence, to avoid having a multiplier effect, a blade count of 51 together with a vane count of 64 were deemed acceptable. This also avoided any multiplier effects with the upstream and downstream counts. If there was a need for better aerodynamic behaviour or to reduce the aerodynamic loading, the blade count could be increased to 53, with a corresponding increase in chord length.

Figure 3 shows the proposed zero-staged rotor compared to the existing two-stage rotor, with the compressor gas path extended and the inlet flared out.
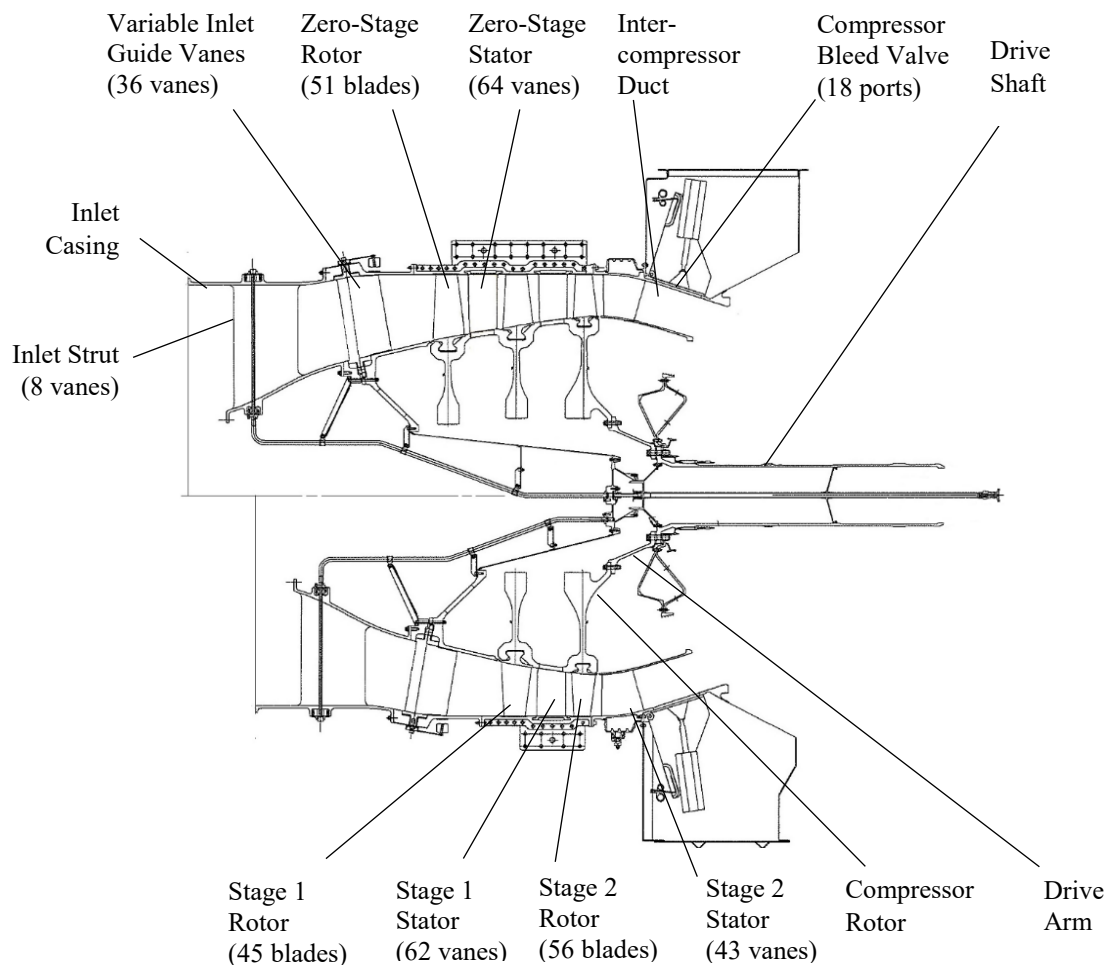
Figure 3. Low Pressure Compressor. Above the Centre-Line: Proposed Zero Stage Design.
Below the Centre-Line: Original Design (Rolls-Royce).

4.8. Airfoil Profile

The next requirement was to define the zero-stage airfoil shapes. The blade entry and exit angle were first determined at the blade mean height from the velocity diagram. Data points from the National Advisory Committee for Aeronautics (NACA) 65-410 blade profile were used. The camber shape was defined as a parabola with the blade maximum thickness at a distance of 40% from the leading edge as specified by the NACA model. From this, the pressure and suction sides were constructed. Figure 4 on the next page shows the method of construction of the airfoil section at the mean blade radius.

Reference point	0	1	2	3	4	5	6	7	8	9	10
y_t (mm)	0	11	22	33	44	55	66	77	88	99	110
x_t (mm)	0	4.02	5.48	6.28	6.60	6.36	5.48	4.16	2.62	1.07	0
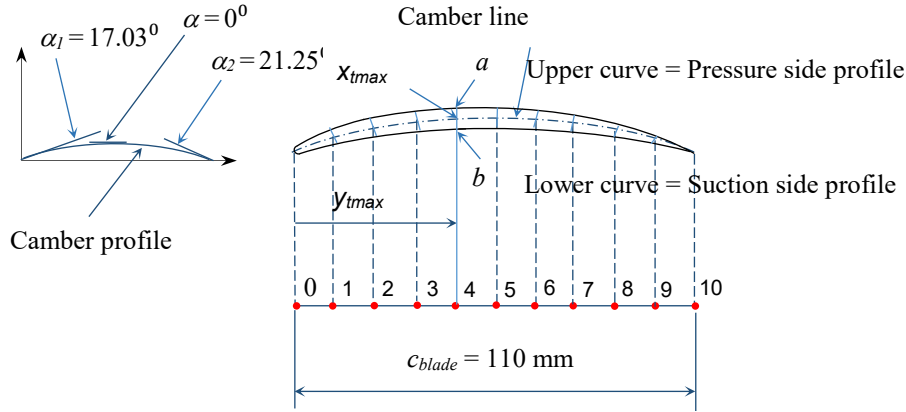
$\alpha_1 = \beta_2 =$ leading edge angle (^{0}). $\alpha_2 = \beta_1 =$ trailing edge angle (^{0}).
$c_{blade} =$ blade chord. $ab =$ blade thickness x_t.
$x_t =$ blade thickness distance ab. $y_t =$ chord distance at x_t.
$y_{tmax} =$ maximum thickness at 40% of $c_{blade} = 110 \times 0.4 = 44$ mm.
$x_{tmax} =$ maximum thickness = 6% of chord length = $110 \times 0.06 = 6.6$ mm.

Figure 4. Construction of Airfoil Surface Coordinates at Mean Blade Radius.

The same calculation was repeated for the entire blade height at one-tenth intervals from hub to tip. This resulted in a series of cross-sections (Table 7). When these were stacked they created the full blade profile. This stacking can be used to create a computerized 3-d solid geometry of the blade for visualization. The same method was applied to define the vane.

These profile images were meant as a first pass. Additional analyses was needed to ensure the most efficient profile possible. Iterations for blade height, chord length, inlet and exit angles, camber and thickness were needed until these converged into a desired airfoil form. Airfoil twist to optimize the flow, and that would affect the inlet and exit angles also needed to be taken into account when finalizing the blade geometry.

After having determined the blade geometry the blade natural frequencies were calculated to ensure there were no resonances with any of the passing frequencies (Table 8) since this would lead to high cycle fatigue and imminent failure. The blade analysis was done using the standard expressions $k = 3\ EI / L3$ and $k = GJ / L$. This was usually calculated for the first six modes. These occurred as a first flex, a first torsion, a second flex, a second torsion, and so on.

The modal frequency results were next superposed on the interference diagram. The interference diagram ensured there were no damaging vibratory interferences across the operating range. This is a standard diagram consisting of the rotor speed range on the horizontal axis, the frequency range at the left vertical axis, and the passing frequency of each interference with each engine order on the right vertical axis. The airfoil mode frequencies were then inserted. Wherever an interference occurred, the rotor speed at the interference was red-flagged as a keep-out zone. That is, the gas turbine could not pause or stop at the interference point, but had to go past it.

The interference diagram identified five interference points for all three modes. These were at 240 rpm, 370 rpm, 620 rpm, 670 rpm and 1,300 rpm. Hence, so long as the compressor did not dwell within these speeds there was no risk of airfoil failure. This requirement was catered for by the logic controller that inhibited the operator from running the gas turbine within this speed range. The actual rotor dwell time for the low pressure compressor when purge speed was attained and light up occurred was 2,800 rpm (Portanier, 2021). This was sufficiently distant from these keep-out zones not to cause any concern. If it was necessary to shift the natural frequency away from an intersection point, this could be done by damping the blade fixing to the disc or by altering the airfoil shape to change its stiffness.

Figure 5 on the next page shows the interference diagram.
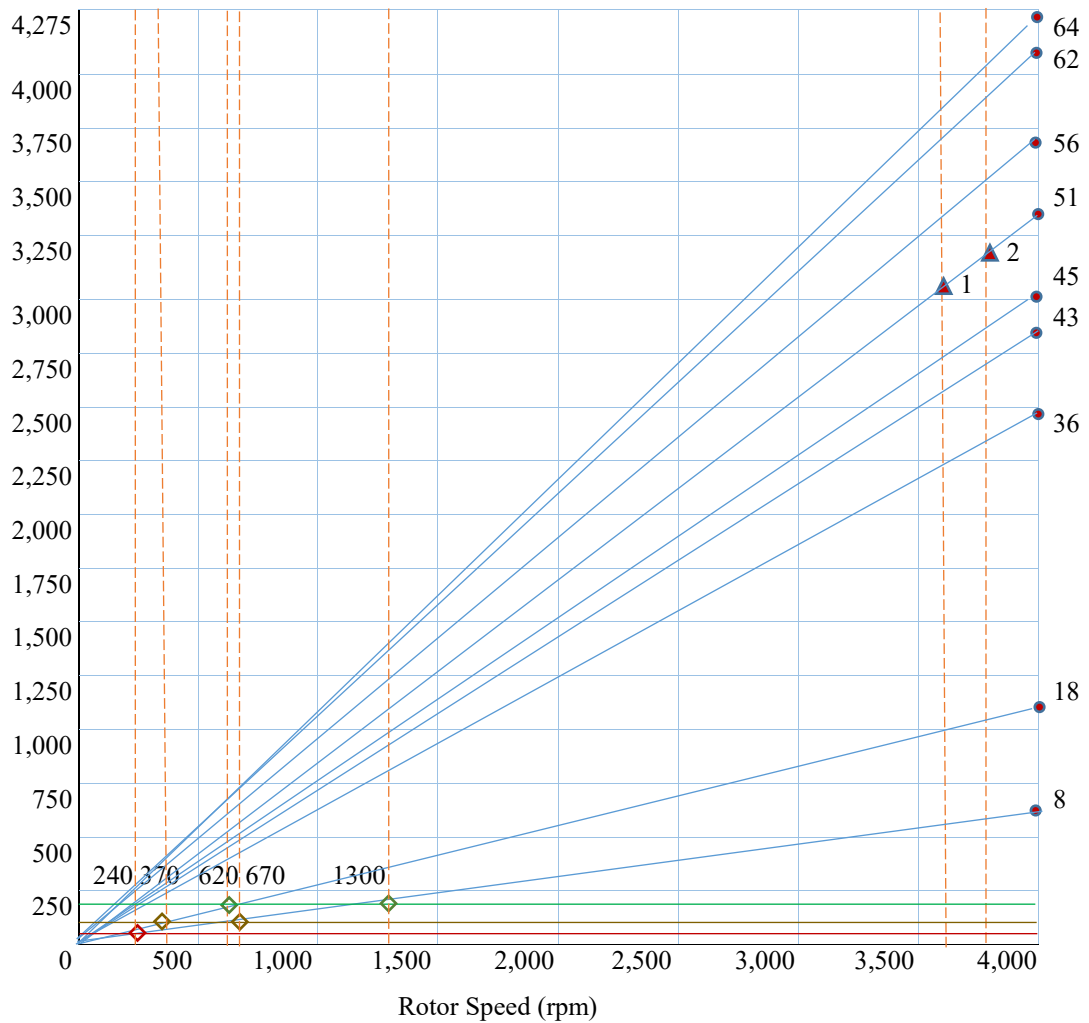
Figure 5. Interference Diagram for the Zero-Stage Blade

4.9. *Combustor Aerothermal Analysis*

The next step investigated the combustor flame temperature as a result of the increase in fuel flow. The higher temperature carried a risk of metal burn. Here, the flame temperature increase could be reduced by:

- Improving the atomization of the fuel in the combustor. Gas turbine manufacturers were continuously developing their fuel nozzle. Hence, when a gas turbine was zero-staged, the latest fuel nozzle design had to be part of the configuration change.
- Increasing the dilution air that mixed with the combustor gas. This reduced the gas temperature as it exited the combustor without reducing the flame temperature.
- Increasing the cooling air to the turbine to reduce the higher temperature on the turbine metal surface.

The amount of additional dilution and cooling air that was needed relative to the combustor temperature was established by determining the increase in blade temperature as a result of the higher power output. This is reviewed in the power output estimation in the next section. The cooling passage and hole-pattern of the blade and vane would also require revising. This was normally done by running the gas turbine under test conditions with the original cooling geometry and carrying out a thermal paint test. The changes in paint colour of the metal surfaces would show the hot spots and where cooling had to be directed.

4.10. Power Output Estimation

The last step in this assessment was to estimate the increase in power output as a result of zero-staging. This was calculated from (Schobeiri, 2016):

$$P = \Delta H / \text{second} = W\, c_p\, \Delta T. \tag{10}$$

Here ΔH = change in enthalpy, W = the mass flow calculated from equation (8), c_p = 1.006 kJ/kg K, and ΔT = the compressor and turbine temperature changes, respectively. Hence, to know the power output required knowing the turbine output less the work done on the compressor. This was found by subtracting the compressor temperature change $\Delta T_{compressor}$ from the turbine temperature change $\Delta T_{turbine}$.

The compressor temperature change was obtained by assuming $T \propto P$ so that:

$$T_2/T_1 = (P_2/P_1)^{(\gamma-1)/\gamma} \tag{11}$$

The turbine temperature change was obtained from the turbine firing temperature and the exhaust temperature calculated from:

$$T_{exhaust} = T_f\,(1/p_r)^{(\gamma-1)/\gamma} \tag{12}$$

where $\gamma = \gamma_{turbine} = 1.33$.

ΔT in equation (10) was expanded to:

$$(T_f - T_{exhaust}) - (T_{compressor} - T_{inlet}). \tag{13}$$

A compressor efficiency of 0.86 and a turbine efficiency of 0.89 were applied. The power output calculation was done for the entire operating range and included the 5% overspeed. The power output at a pressure ratio of 34.3, that is, without zero-staging, came to 63.73 MW. For a pressure ration of 36.5, that is, with zero-staging, the power output came to 73.77 MW. With a 5% overspeed, this came to 88.1 MW (Table 9).

The gas turbine manufacturer's data sheet rated the power output at a pressure ratio of 34.3 as 57.9 MW. The calculated power output for the same condition was 9% more that the gas turbine manufacturer's rating. The rating as specified on the data sheet was guaranteed and the calculated power output was adjusted to correspond with this. A reverse calculation using 57.9 MW gave a turbine firing temperature of T_f = 1,667 K instead of the originally calculated temperature of 1,731 K. The power output was re-calculated using the lower firing temperature. This gave a zero-stage power output of 67.76 MW and an overspeed power output of 80.87 MW (Table 10). Using this power output permitted determining the combustor and turbine temperatures by working backwards (Table 11). In turn, the temperature increase was found (Table 12). This would help determine the additional cooling air.

A final verification was needed to ascertain sufficient surge margin. Reference was made to the compressor map (Figure 2) and the surge margin relative to the power output over the entire operating range showed it to be sufficient up to the 5% overspeed.

In a similar manner, the power output was plotted against the rotor speed along the entire operating range from idle to 5% overspeed to ascertain its validity. The standardized rotor speed of 3,570 rpm at 100% speed was used as the base load reference. The plot showed that the power output increase was typical for any mechanical drive gas turbine and followed the typical cube law curve with $P \propto N^3$ and with its shape in agreement with Cohen et al. (1972) and Ko et al. (2005).

4.11. Logic Controller Assessment

The zero-stage addition also required revising the controller logic limits and trips that regulated safe operation of the gas turbine. Here, the parametric values for the higher pressures and higher temperatures needed correlating with those for the increase in fuel flow, rotor speed and power output. The fuel flow governed the power output, while the temperature, pressure and rotor speed were limiting factors for safe operation.

The rate of acceleration at start-up was regulated by the increase in fuel flow, and with rotor stability monitored by measuring shaft speed. The higher compressor working line also had an impact on the surge margin during start-up, at transients and for peak power. The surge margin was safeguarded by modulating the variable inlet guide vanes and bleed valves to control the mass-flow. The transient sequence also had to be considered, with relight time extended in case of flame out to prevent shut down. The stop sequence deceleration rate remained

unchanged. The low pressure rotor lower limit that was originally set at 680 rpm based on the rotor achieving speed stability, was now reset to 720 rpm to prevent the rotor from dwelling below this speed. Keep-out zones that had to be considered but not addressed here were the critical speeds of driven equipment. These were typically the reduction gear box, electrical generator and propeller drive. Any deviation from the prescribed settings would result in an annunciation to the logic controller to initiate remedial action either as a power pull-back or a shutdown. The logic controller model for regulating gas turbine behaviour is summarized by the diagram shown in Figure 6 (Portanier, 2021).
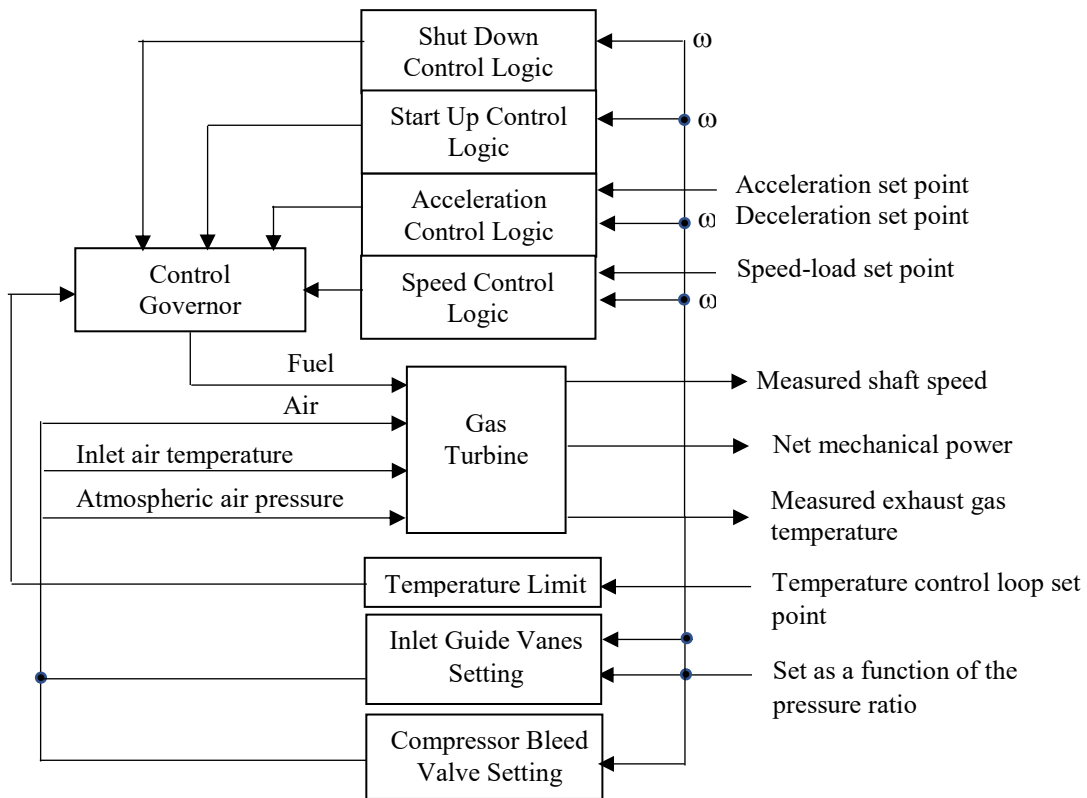
Figure 6. Gas Turbine Logic Controller Diagram

5.   Conclusion

Zero-staging The Trent 60 mechanical drive configuration as a medium-sized aero-derivative gas turbine with its inherently high rotational speed and high thermal efficiency proposed an increase in the compressor pressure ratio from 34.3 to 36.5 or by 5%, resulting in an increase in mass flow from 157.7 kg/second to 185.3 kg/second or by 27.6 kg/second, and an increase in exhaust temperature from 447 C to 458 C or by 11 C. This raised the thermal efficiency from 42.4% to 44.4%, or by 2%, and increased the power output from 57.9 MW to 67.76 MW, or by 17%.

These results were based on simple equations and scaling and were meant as a first pass assessment to map the compressor, calculate the firing temperature and estimate the power output. Notwithstanding that the approach was simplistic and used simplifying assumptions, the results appeared credible because they gave the expected outcome. However, further verification was needed to validate the method. One approach would consist of redoing the same calculations on a different gas turbine configuration for comparison.

References

Boyce, Meherwan. 2011. The Gas Turbine Engineering Handbook. 2ed. Butterworth-Heinemann Oxford. UK.

Boyce, Meherwan. 2006. The Gas Turbine Engineering Handbook. Chapter 2. Axial-Flow Compressors. National Energy Technology Laboratory.

Boyce, Meherwan. 2002. Gas Turbine Engineering Handbook, 2ed. Gulf Professional Publishing: Boston.

Boyce, Meherwan. 1967. Design of Compressor Blades Suitable for Transonic Axial Flow Compressors. The American Society of Mechanical Engineers. 67-GT-47.

Cohen, H. G.F.C. Rogers and H.I.H. Saravanamuttoo. 1972. Gas Turbine Theory. Longman: London.

EASA. Type-Certificate Data Sheet No. E.047, 2019. https://www.easa.europa.eu/. Accessed 18 August 2020.

Jackson, A. J. B. 2009. Optimization of Aero and Industrial Gas Turbine Design for the Environment. PhD Thesis. Cranfield University.

Ko, Henry. Scott Nolen. Kevin Goom. 2005. Trent 60 Design and Validation for Mechanical Drive Service. Industrial Applications of Gas Turbines Committee Paper No: 05-IAGT-1.4.

National Advisory Committee for Aeronautics. Airfoil Database NACA 6 series. NACA 65-410. http://airfoiltools.com/. Accessed 12 Dec 2020.

Portanier, Ronald. 2021. The Aero-derivative Gas Turbine as a Marine Propulsion Engine: Defining a More Competitive Marine Gas Turbine with a Step-Change Increase in Power Rating by Zero-Staging the Compressor. Thesis. MSc Engineering for Marine Professionals. MLA College with the University of Plymouth. UK.

Schobeiri, Meinhard T. 2016. Gas Turbine Design, Components and System Design Integration. Springer. New York.

Walsh, Philip and Paul Fletcher. 2004. Gas Turbine Performance, Blackwell: Oxford. UK.

Spreadsheet Tabulations

Table 1. Temperature Comparisons between the Aero-Fan Trent and the Aero-Derivative Trent

Station	Aero-Fan Trent (K)	Trent 60 (K)	Difference (K)	Difference %
Compressor exit temperature	910	873	-37	-4.1
Combustor outlet temperature	1,794	1,721	-73.5	-4.1
Turbine firing temperature	1,692	1,622	-70	-4.1
Turbine exhaust temperature	843	720	-123	-14.5

Table 2. Increase in Turbine Firing Temperature and Thermal Efficiency

Turbine Firing Temperature T_f (K)	Turbine Firing Temperature Increase (K)	Pressure Ratio r_p	Pressure Ratio Increase	Thermal Efficiency n_{cycle} (%)
1,815	30	38.1	1.11	46.8
1,785	30	37.7	1.10	46.4
1,755	30	37.1	1.08	46.0
1,725	30	36.5	1.06	45.6
1,695	30	35.8	1.05	45.1
1,665	30	35.2	1.03	44.6
1,635	12	34.6	1.01	44.2
1,622	Baseline	34.3	1.00	43.9

Table 3. Calculated Gas Turbine Thermal Efficiency

Turbine Firing Temperature T_f (K)	Compressor Pressure Ratio p_r	Thermal Efficiency %
1,815	38.1	46.79
1,785	37.7	46.41
1,755	37.1	45.99
1,725	36.5	45.56
1,695	35.8	45.11
1,665	35.2	44.64
1,635	34.6	44.15
1,622	34.3	43.93
1,605	33.9	43.63
1,575	33.3	43.10
1,545	32.7	42.54
1,365	28.8	38.56
1,185	25.1	32.28
1,005	21.2	20.79
945	19.9	12.21
885	18.7	7.01

Table 4. Increase in Flow Relative to Pressure Ratio

Flow Coefficient Q	Pressure Ratio r_p	Compressor Pressure P (kPa)	Compressor Temperature T (K)	Mass Flow W (kg/second)
1.50	38.1	3,858.46	900.96	192.8
1.48	37.7	3,794.62	896.45	187.0
1.45	37.1	3,730.79	891.89	181.2
1.43	36.5	3,666.95	887.27	175.5
1.40	35.8	3,603.12	882.60	169.9
1.38	35.2	3,539.28	877.86	164.4
1.35	34.6	3,502.81	875.13	160.0
1.34	34.3	3,475.45	873.07	157.7

Table 5. Compressor Aerodynamic Tabulation at Sea Level Conditions

Stage Reference Number	Mach Number	V (metres/ second)	A (m²)	W (kg/ second)	$W \sqrt{T}/P$ (kg/second K / kPa)	Flow Function Q_c /Q
1	0.06	20	0.445	10.90	1.83	1.00
2	0.12	40	0.445	21.81	3.65	2.00
3	0.18	61	0.445	33.25	5.57	3.05
4	0.24	81	0.445	44.16	7.40	4.05
5	0.29	98	0.445	53.42	8.95	4.90
6	0.35	119	0.445	64.87	10.87	5.95
7	0.41	139	0.445	75.77	12.69	6.95
8	0.47	159	0.445	86.67	14.52	7.95
9	0.53	180	0.445	98.12	16.44	9.00
10	0.59	200	0.445	109.03	18.26	10.00
11	0.65	221	0.445	120.47	20.18	11.05
12	0.71	241	0.445	131.38	22.01	12.05
13	0.76	258	0.445	140.64	23.56	12.90
14	0.82	279	0.445	152.09	25.48	13.95
15	0.88	299	0.445	162.99	27.31	14.95
16	0.94	319	0.445	173.89	29.13	15.95
17	1.00	340	0.445	185.34	31.05	17.00
18	1.06	360	0.445	196.25	32.88	18.00

Table 6. Stage Reference Number to Compressor Pressure Ratio and Rotor Speed

Stage Reference Number	Pressure Ratio p_r	Compressor Exit Pressure P (kPa)	Compressor Calculated Exit Temperature T (K)	Compressor Adjusted Exit Temperature T (K)	Rotor Speed N (rpm)	Corrected Rotor Speed $N/\sqrt{T}$
1	2.1	214.57	368.26	375.62	210	12.37
2	4.2	429.14	459.18	468.37	420	24.74
3	6.3	643.71	521.34	531.77	630	37.11
4	8.5	858.28	570.03	581.43	840	49.48
5	10.6	1,072.85	610.64	622.85	1,050	61.86
6	12.7	1,287.42	645.80	658.72	1,260	74.23
7	14.8	1,501.99	676.99	690.53	1,470	86.60
8	16.9	1,716.56	705.14	719.25	1,680	98.97
9	19.1	1,931.14	730.88	745.50	1,890	111.34
10	21.2	2,145.71	754.69	769.78	2,100	123.71
11	23.2	2,360.28	776.74	792.27	2,310	136.08
12	25.4	2,574.85	797.50	813.45	2,520	148.45
13	27.5	2,789.42	817.05	833.39	2,730	160.82
14	29.6	3,003.99	835.56	852.27	2,940	173.20
15	31.7	3,218.56	853.06	870.12	3,150	185.57
16	33.9	3,433.13	869.83	887.23	3,360	197.94
17	36.5	3,647.70	885.87	903.59	3,570	210.31
18	38.1	3,862.27	901.24	919.27	3,748	220.82

Table 7. Basic Profile Shapes for the Zero-Stage Blade

Blade Height	Inlet angle α_1 (^{0})	Exit angle α_2 (^{0})	Blade Section Profile
100%	6.41	8.80	
90%	7.51	10.12	
80%	8.86	11.72	
70%	10.70	13.89	
60%	13.26	16.89	
50%	17.03	21.25	
40%	23.03	28.00	
30%	33.59	39.31	
20%	54.15	59.28	
10%	70.90	73.90	

Table 8. Low Pressure Compressor Engine Orders with Passing Frequencies at 100% Rotor Speed

Component	Count	Passing Frequency (Hz)
Inlet Struts	8 Vanes	476
Variable Inlet Guide Vanes	36 Vanes	2,142
Zero Stage Rotor	51 Blades	3,034
Zero Stage Stator	64 Vanes	3,808
Stage 1 Rotor	45 Blades	2,677
Stage 1 Stator	62 Vanes	3,689
Stage 2 Rotor	56 Blades	3,332
Inter Compressor Duct	43 Vanes	2,558
Low Pressure Bleed Off Valve	18 Ports	1,071

Table 9. Calculated Power Output

Pressure Ratio p_r	T_{inlett} (K)	$T_{compressor}$ (K)	$\Delta T_{compressor}$ (K)	T_f (K)	$T_{exhaust}$ (K)	$\Delta T_{turbine}$ (K)	$P= W\, c_p\, \Delta T$ (MW)
38.1	288.15	919.59	631.44	1924	779.63	1,144.37	88.10
36.5	288.15	903.59	615.44	1817	746.80	1,070.20	73.77
34.3	288.15	892.34	599.08	1731	720.04	1,010.96	63.73
33.9	288.15	887.23	564.56	1710	713.49	996.51	60.49
31.7	288.15	870.12	545.24	1603	679.65	923.35	48.70
29.6	288.15	852.71	564.56	1497	645.63	851.37	38.18
27.5	288.15	833.39	504.12	1390	610.62	779.38	28.82
25.4	288.15	813.46	481.63	1283	574.93	708.07	21.01
23.3	288.15	792.27	457.32	1176	538.50	637.50	14.06
21.2	288.15	769.78	431.10	1069	501.17	567.83	13.05
19.1	288.15	745.47	402.38	962	462.97	499.03	3.10
16.9	288.15	719.25	370.57	855	423.69	431.31	0.58
14.8	288.15	690.53	334.7	748	383.17	364.83	-1.22

Table 10. Comparison of Calculated and Adjusted Shaft Power Output and Rotor Speed

Pressure Ratio (p_r)	Initial Firing Temperature T_f (K)	Calculated Net Power P (MW)	Adjusted Firing Temperature T_f (K)	Adjusted Net Power P (MW)	Rotor Speed N (rpm)
38.1	1,924	88.1	1,853	80.87	3,748
36.5	1,817	73.7	1,750	67.76	3,570
34.3	1,731	63.73	1,667	57.90	3,401
33.9	1,710	60.49	1,647	54.91	3,360
31.7	1,603	48.70	1,544	43.86	3,150
29.6	1,497	38.18	1,441	34.01	2,940
27.5	1,390	28.82	1,338	25.29	2,730
25.4	1,283	21.01	1,235	18.02	2,520
23.3	1,176	14.06	1,132	11.59	2,310
21.2	1,069	13.05	1,029	11.05	2,100
19.1	962	3.10	926	2.98	1,890
16.9	855	0.58	823	0.56	1,680
14.8	748	-1.22	720	-1.17	1,470

Table 11. Power Output Reference to Temperature Increases

Power Output Reference	Pressure Ratio r_p	P (MW)	$T_{combustor}$ (K)	T_{firing} (K)	ΔT (K)	Increase in $T_{combustor}$ (K)	Increase in T_{firing} (K)
Baseline	34.3	57.90	1,766	1,667	99.19	Baseline	Baseline
Zero-stage	36.5	67.76	1,854	1,750	104.13	87.94	83.00
5% peak	38.1	80.87	1,963	1,853	110.26	109.13	103.00

Table 12. Blade Relative Temperature without and with Zero-Staging

Power Output Reference	T_{blade} (K)	T_{cr} (K)	T_g (K)	$T_{dynamic}$ (K)	Air velocity (m/sec)	C_p (kJ/kg K)	Blade Relative Temperature	Increase (%)
Baseline	1,731	873	1,658	923.65	319	1.006	1.093	–
Zero Stage	1,817	885	1,687	943.33	340	1.006	1.161	6.27